Journal of Power Sources 191 (2009) 591–600

Contents lists available at ScienceDirect

Journal of Power Sources

journal homepage: www.elsevier.com/locate/jpowsour

Sucrose-aided combustion synthesis of nanosized $LiMn_{1.99-y}Li_yM_{0.01}O_4$ ($M = Al^{3+}$, Ni^{2+}, Cr^{3+}, Co^{3+}, $y = 0.01$ and 0.06) spinels Characterization and electrochemical behavior at 25 and at 55 °C in rechargeable lithium cells

J.M. Amarilla [a], K. Petrov [b], F. Picó [a], G. Avdeev [b], J.M. Rojo [a], R.M. Rojas [a,*]

[a] Instituto de Ciencia de Materiales de Madrid, Consejo Superior de Investigaciones Científicas (CSIC), Sor Juana Inés de la Cruz no. 3, Cantoblanco, 28049 Madrid, Spain
[b] Institute of General and Inorganic Chemistry, Bulgarian Academy of Sciences, 1113 Sofia, Bulgaria

ARTICLE INFO

Article history:
Received 12 September 2008
Received in revised form 4 February 2009
Accepted 7 February 2009
Available online 20 February 2009

Keywords:
$LiMn_2O_4$
Combustion synthesis
Li-ion batteries
Spinels
High temperature cycling behavior

ABSTRACT

Doubly doped $LiMn_{1.99-y}Li_yM_{0.01}O_4$ ($M = Al^{3+}$, Ni^{2+}, Cr^{3+}, Co^{3+}; $y = 0.01$ and 0.06) spinels have been synthesized by the sucrose-aided combustion method. Combined TG/DTA and XRD studies have shown that stoichiometric single-phase spinels are formed after annealing of the samples at 700 °C for 1 h. The samples obtained are nanocrystalline materials having a narrow size-distribution and a coherent domain size between 40 and 60 nm, depending on the amount of fuel (sucrose) used in the synthesis. The influence of the Li-excess, the type of M^{n+}-dopant cation and the amount of fuel used in the synthesis on the electrochemical behavior of the spinels in a Li-cell at room and at elevated temperature (55 °C) has been studied. At 25 °C all the spinels synthesized have a good capacity retention after 100 cycles, QRt-100 > 92%. At 55 °C the increase of the Li-excess improves the cycling performances. Rate capability studies show that the spinels retain >90% of their capacity even at 5*C* rate. The synergic effect of the Li-excess and the particle size on the electrochemical properties of the spinels as cathode material has been settled. The $LiMn_{1.93}Li_{0.06}M_{0.01}O_4$, ($M = Al^{3+}$, Ni^{2+}) spinels, with cyclabilities >99.9% by cycle at both 25 and 55 °C, and high rate capabilities, are the ones that show the best electrochemical properties.

1. Introduction

Several manganese oxides have been considered as electrode materials for various types of batteries, including rechargeable lithium ion batteries [1,2]. Among them, lithium manganese oxide spinel $LiMn_2O_4$ is particularly attractive as a promising positive electrode active material, hereafter named cathode material, for the new generations of Li-ion batteries. It is a mixed ionic–electron conductor that intercalates reversibly Li^+ ions at about 4 V [3]. The $LiMn_2O_4$ itself is cheap, non-toxic and can be easily prepared. However it shows a capacity fade on cycling at room temperature, and a more severe one at high temperature, ≈50 °C [4–10]. Causes of the capacity fade are so far complex and several reasons have been given to account for it, among them: (i) dissolution of Mn^{2+} formed by the disproportionation reaction $2Mn_{(solid)}{}^{3+} \rightarrow Mn_{(solid)}{}^{4+} + Mn_{(solution)}{}^{2+}$ due to the acid attack of the HF generated by hydrolysis of the $LiPF_6$ of the electrolyte [1,5–8]; (ii) the onset of the Jahn–Teller effect at the end of the discharge on the surface of the particles [8]; (iii) mechanical instability generated by structural changes occurring during Li^+-de/insertion in the charge/discharge steps [9,10]. It is possible that the three phenomena contribute simultaneously to the capacity fade of the $LiMn_2O_4$ electrode. It has been shown that doping with several foreign cations such as Li^+, Ni^{2+}, Al^{3+}, Cr^{3+}, Co^{3+}, etc. improves the cycling performances of the $LiMn_2O_4$-based electrodes [1,10–15]. In fact, substitution for Mn^{3+} by other metals decreases the dissolution of the $LiMn_2O_4$-based spinels [7,16], suppresses the Jahn–Teller effect [17–20] and reduces the volume difference between the charged/discharged structures of the doped spinel [9,10,12]. Recently, it has been demonstrated that double doping, particularly when Li^+ is one of the doping cations, improves the cycling performance of the $LiMn_2O_4$-based cathodes [10,21].

For practical applications, high rate capability is one of the most important characteristics of electrode materials. It has been shown that nanostructured electrodes are able to drain high capacity at high currents, because diffusion path of Li^+ in the solid is significantly smaller than in electrodes of the same materials but with higher particle size [22–27]. We think that it is plausible to assume that to develop doubly doped spinels with nanometer size would

* Corresponding author. Fax: +34 91 3720623.
E-mail address: rmrojas@icmm.csic.es (R.M. Rojas).

0378-7753/$ – see front matter © 2009 Elsevier B.V. All rights reserved.
doi:10.1016/j.jpowsour.2009.02.026

be helpful in improving both the rate capability and the cyclability of the cathodes.

Aimed to obtain $LiMn_2O_4$-based cathodes for Li-ion batteries with high electrochemical performances both at 25 and 55 °C, we have synthesized nanosized doubly doped $LiMn_{1.99-y}Li_yM_{0.01}O_4$ spinels with two different Li-excess content, $y = 0.01$ and 0.06. Several M^{n+}-dopant cations ($M = Al^{3+}$, Ni^{2+}, Cr^{3+}, Co^{3+}) has been tested out. The samples have been obtained by an original, competitive, cheap and straightforward sucrose-aided combustion method that affords homogeneous and single phase compounds. The samples obtained have been characterized by X-ray powder diffraction (XRD), differential and thermogravimetric analysis (DTA/TG) and transmission electron microscopy (TEM). The influence of the Li-excess, the M^{n+}-dopant cation and the amount of fuel used in the combustion synthesis on the electrochemical behavior of the spinels in a lithium cell at room and at elevated temperature (55 °C) has been studied.

2. Experimental

The $LiMn_{1.99-y}Li_yM_{0.01}O_4$ ($M = Al^{3+}$, Ni^{2+}, Cr^{3+}, Co^{3+}, $y = 0.01$ and 0.06) spinels have been synthesized by the sucrose-aided combustion method [22], from reagent grade Li_2CO_3, $Ni(NO_3)_2{\cdot}6H_2O$, $Al(NO_3)_3{\cdot}9H_2O$, $Co(NO_3)_2{\cdot}6H_2O$ and $Cr(NO_3)_3{\cdot}9H_2O$. Mn metal dissolved in 0.25 M HNO_3 was used as manganese source. Preset amounts of dried Li_2CO_3 were dissolved in a small amount of diluted HNO_3 to avoid vigorous evolution of CO_2. A stoichiometric amount of the previously dissolved Mn was added to the Li-containing solution. Then, solutions of the corresponding metal nitrates with predetermined M^{2+} or M^{3+} content were dropped into the Mn and Li containing solution, with a graduated micropipette having an accuracy of 0.001 ml. Finally, the necessary amount of sucrose dissolved in the minimum amount of water was added. The formal chemical equation that describes the combustion in a closed system, and allows determination of the amount of sucrose, w, needed to obtain 1 mol of the spinel product is[1]:

$$(1+y)LiNO_3 + zM^{n+}(NO_3)_n + (2-y-z)Mn(NO_3)_2 + wC_{12}H_{22}O_{11} \rightarrow LiMn_{2-y-z}Li_yM_zO_4 + 12wCO_2 + 11wH_2O + 1/2[5-y+(n-2)z]N_2 \quad (1)$$

The stoichiometric amount of sucrose, w, can be deduced from the oxygen mass balance from Eq. (1) as follows:

$$3(1+y) + 6z + 6(2-y-z) + 11w = 4 + 24w + 11w;$$
$$w = \frac{(11-3y)}{24}; \quad \text{for } M = M^{2+} \quad (2)$$

$$3(1+y) + 9z + 6(2-y-z) + 11w = 4 + 24w + 11w;$$
$$w = \frac{(11-3y+3z)}{24}; \quad \text{for } M = M^{3+} \quad (3)$$

It has been found earlier [22–24,28] that when the stoichiometric amount of sucrose, w, is used the reaction is very violent and the product blows up out of the reaction vessel. However, the process can be easily controlled by increasing the relative amount of sugar. In our case, in the synthesis of Ni^{2+} and Al^{3+}-doped samples the amount of sucrose used was $1.5w$, and for Cr^{3+} and Co^{3+} this amount was $3w$. It also allowed us to investigate if of the amount of fuel affects the characteristics and properties of the synthesized spinels. The reagents solutions were heated at about 120 °C for ≈30 min and when dried they start to swell up due to the evolution of gases generated during thermolysis of the reagents, giving way to a foamy mass. After a few minutes, the mass starts to burn up spontaneously without flame. The product of the reaction is a very light and fluffy black powder. The yield of the reaction is ≈98%. Samples once obtained were heated at 400 °C for 1 h. These samples will be hereafter referred to as "as prepared". Undoped-$LiMn_2O_4$ used as reference, has been synthesized by the same combustion synthesis procedure, using 3w fuel. All the "as-prepared" samples were treated in air at 700 °C for 1 h, at a heating/cooling rate of 2 °C min^{-1}.

The phase purity and morphology of the samples were studied by X-ray powder diffraction. XRD patterns were recorded at room temperature in a Bruker D8 diffractometer, with CuKα radiation. The patterns were obtained in the step scanning mode at 0.02° (2θ) step and 1 s step^{-1} counting time, within the range $10° \leq 2\theta \leq 80°$. Lattice parameters were refined with the CELREF program [29]. The average crystallite size was calculated from several diffraction lines from the Scherrer formula $D = \lambda/\beta\cos\theta$, where λ is the wavelength of CuKα = 1.54186 Å, θ is the diffraction angle, and $\beta = \sqrt{(\beta_m^2 - \beta_s^2)}$ is the corrected half-width of the diffraction peaks, where β_m is the observed half-width of the experimental diffraction peaks, and β_s is the half-width of the diffraction peaks of a standard sample, in our case an Al_2O_3 flat-plate of the National Institute of Standards Technology (NIST).

Differential (DTA) and thermogravimetric (TG) analysis were carried out simultaneously with a Stanton STA 781 instrument up to 1000 °C in still air, and 10 °C min^{-1} heating and cooling rates. About 30 mg of sample was used in each run, and α-Al_2O_3 was the inert reference. The instrument was calibrated with certified reference materials from NIST.

Transmission electron (TEM) micrographs were taken in a JEOL JEM1010 electron microscope operating at an acceleration voltage of 100 kV. The samples were dispersed in *n*-butyl alcohol, and drops of the dispersion were transferred to a holey carbon-coated copper grid.

Electrochemical studies were performed at 25 and at 55 °C on all the 700 °C-heated $LiMn_{1.99-y}Li_yM_{0.01}O_4$ ($M = Al^{3+}$, Ni^{2+}, Cr^{3+}, Co^{3+}; $y = 0.01$, 0.06) spinels in CR2032 coin cells. Positive electrode composites were prepared from the spinel powder (≈20 mg or 72 wt.%), MMM Super P carbon black (17 wt.%) and a plasticizer (Kynar Flex® 2801, 11 wt.%). These percentages were chosen in accordance with those reported by Lazarraga et al. [30]. We proceeded as follows: 3 ml of acetone was added to the mixture of the three solid components, and it was stirred for 3 h. The solvent was allowed to evaporate at room temperature, and then kept at 80 °C for 2 h. Cylindrical pellets of composite (12 mm diameter and ca. 0.2 mm thickness) of positive electrode were obtained after cold pressing at 370 MPa. The negative electrode was a lithium foil, which also operated as reference electrode. The electrodes were separated by a Whatman BSF80 paper soaked in the electrolyte, 1 M solution of $LiPF_6$ in ethylene carbonate and dimethyl carbonate (EC/DMC 1:1) electrolyte (as supplied by UBE). The components were assembled into the coin cell within an argon glove box in which water content was kept below 1 ppm. Cycle tests were carried out between 4.2 and 3.4 V at both 25 and at 55 °C at high current rates: 0.5*C* rate in charge ($j \approx 1.3$ mA cm^{-2}) and at 1*C* rate in discharge ($j \approx 2.6$ mA cm^{-2}) with an Arbin battery tester system (BT2043). *C* is the capacity of the cathode calculated from the theoretical capacity of the spinel and the mass of spinel used in the composite. The *C* coefficient is the inverse of the theoretical charge/discharge time in hours. The rate capability measurements have been investigated by discharging from 0.2*C* to 5*C* between 3.1 and 4.4 V at room temperature. Charging was done at 0.5*C* for all the discharge rates used except when discharging was done at 0.2*C*. In this case, charging was done at 0.2*C*.

[1] To bring calculations into general use the $LiMn_{2-y-z}Li_yM_zO_4$ formula has been used. In our samples, z = 0.01.

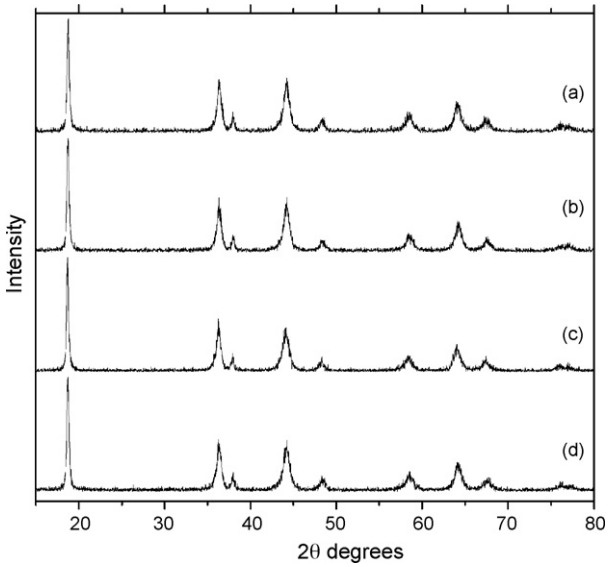

Fig. 1. Room temperature XRD patterns of some $LiMn_{1.99-y}Li_yM_{0.01}O_4$ spinels "as prepared": (a) $LiMn_{1.98}Li_{0.01}Ni_{0.01}O_4$, (b) $LiMn_{1.93}Li_{0.06}Ni_{0.01}O_4$, (c) $LiMn_{1.98}Li_{0.01}Al_{0.01}O_4$, (d) $LiMn_{1.93}Li_{0.06}Al_{0.01}O_4$.

3. Results and discussion

3.1. Structural, thermal and morphological characterization

The XRD patterns obtained for the "as prepared" samples are practically identical. They show broad diffraction lines, which can be fully indexed in the *Fd*3*m* space group. As an example, patterns recorded for the $LiMn_{1.99-y}Li_yM_{0.01}O_4$ (M = Ni^{2+}, Al^{3+}; $y = 0.01$ and 0.06) spinels are presented in Fig. 1. Values of lattice parameter, a_c, determined for these samples are summarized in Table 1. Lattice parameters determined for the Cr^{3+} and Co^{3+}-doped spinels are slightly larger than those determined for the Ni^{2+} and Al^{3+}-doped samples, and they decrease slightly on increasing the amount of lithium in the spinel. The crystallite sizes determined for the "as prepared" samples is ≈20 nm, being them also somewhat higher for the Cr^{3+} and Co^{3+}-doped samples than for the Ni^{2+} and Al^{3+} ones, the former being synthesized with larger amount of fuel (3*w*) than the latter (1.5*w*).

Thermal analysis curves recorded for all the "as prepared" samples are similar. As an example, DTA/TG curves recorded simultaneously for the "as prepared" $LiMn_{1.93}Li_{0.06}Ni_{0.01}O_4$ spinel are presented in Fig. 2a. Between room temperature and ≈200 °C the DTA curve shows two small endothermic peaks, which correspond with a small weight loss in the TG curve, ≈0.5%. These effects can be attributed to the removal of some humidity in the sample. After that and at ≈300 °C a broad exothermic peak appears in the DTA curve. It can be ascribed to the combustion of some organic amorphous impurities [23,24,28]. These impurities, which are not detectable by XRD, indicate that the "as prepared" samples are not pure spinels even after being thermally treated at 400 °C for 1 h. However, it is worth to mention that the exothermic effect is very small and hence, the amount of impurities must be very low. In the TG curve and between ≈380 and 680 °C (marked A, B in Fig. 2a), a smooth and continuous weight loss of ≈0.5% as well as a plateau between 680 and 720 °C (marked B, C in Fig. 2a) are observed. As it can be seen in Fig. 2b, in which TG curves recorded for the four "as prepared" $LiMn_{1.93}Li_{0.06}M^{n+}{}_{0.01}O_4$ are presented, the samples containing Cr^{3+} or Co^{3+} (marked A′, B′ in Fig. 2b) undergone in this temperature interval a smaller weight loss, ≈0.2%, than the Ni^{2+} and Al^{3+} (A, B in Fig. 2b) doped samples, ≈0.5%. It has been reported that the spinels obtained at low temperature are cation deficient [31–33],

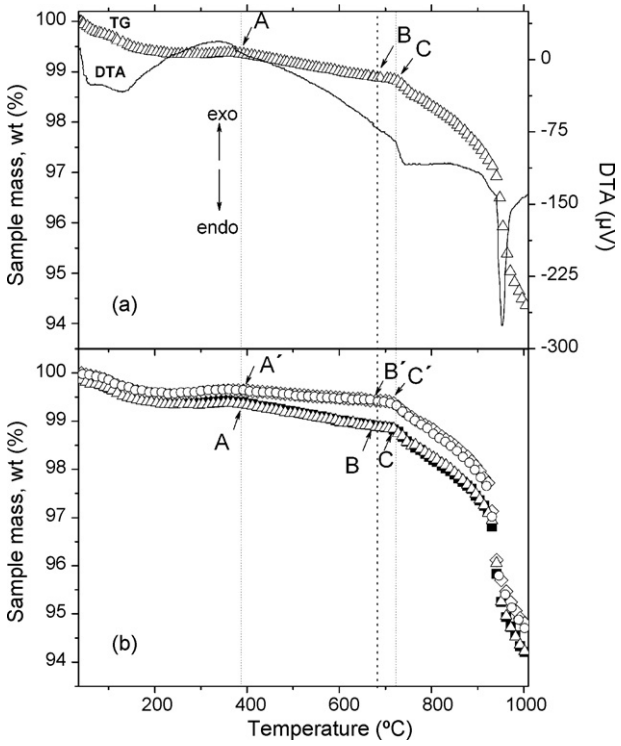

Fig. 2. (a) DTA/TG curves recorded for the $LiMn_{1.93}Li_{0.06}Ni_{0.01}O_4$ "as prepared"; (b) TG curves recorded for the $LiMn_{1.93}Li_{0.06}M^{n+}{}_{0.01}O_4$, M = Ni^{2+} (△), Al^{3+}(■), Cr^{3+} (◊), Co^{3+} (○).

and on heating the stoichiometry adjusts leading to the formation of the stoichiometric spinels. This small weight loss process, which is not accompanied by any thermal effect in the DTA curve, can be hence assigned to the adjustment of the spinels stoichiometry. The number of cation defects in the non-stochiometric spinels can be determined assuming that: (i) the spinels with the stoichiometric compositions are formed in the plateaus observed in the TG curves between 680 (marked B, B′ in Fig. 2a and b) and 720 °C (marked C, C′ in Fig. 2a and b); (ii) between ≈385 °C (marked A, A′ in Fig. 2a and b) and ≈680 °C (marked B, B' in Fig. 2a and b) the process undergone by the spinels can be described by the following equation:[2]

$$\boldsymbol{a}Li_uM_v^{n+}Mn_xO_4 \xrightarrow{385^{o}-680^{o}C} \boldsymbol{b}LiMn_{2-y-z}Li_yM_zO_4 + \boldsymbol{c}O_2$$

$$(M = Al^{3+},\ Ni^{2+},\ Cr^{3+},\ Co^{3+},\ y = 0.01,\ 0.06,\ z = 0.01) \quad (4)$$

From the molecular weight of the stroichiometric spinels, the number of moles of spinel, **b**, formed at the temperatures B and B′ and present between 680 and 720 °C (Fig. 2) can be determined. From the mass difference between A and B, and between A′ and B′, the moles of oxygen evolved, **c**, can also be determined. Accepting that the non-stoichiometry in the spinels is due to cation deficiency and that the oxygen content is kept constant and equal to four, the following relationship can be proposed:

$$4\boldsymbol{a} = 4\boldsymbol{b} + 2\boldsymbol{c} \quad (5)$$

By applying the above indicated relationships to the TG curves recorded for the $LiMn_{1.93}Li_{0.06}M^{n+}{}_{0.01}O_4$ spinels (M^{n+} = Al^{3+}, Ni^{2+}, Cr^{3+} and Co^{3+}) the following equations have been derived:

$$Li^{+}{}_{1.043}Al^{3+}{}_{0.0098}Mn^{3+}{}_{0.668}Mn^{4+}{}_{1.231}O_4$$

$$\xrightarrow{\Delta} 0.984Li^{+}{}_{1.06}Al^{3+}{}_{0.01}Mn^{3+}{}_{0.81}Mn^{4+}{}_{1.12}O_4 + 0.032O_2 \quad (6)$$

[2] To bring calculations into general use the $LiMn_{2-y-z}Li_yM_zO_4$ formula has been used. In our samples, z = 0.01.

$$Li^{+}_{1.044}Ni^{2+}_{0.0098}Mn^{3+}_{0.668}Mn^{4+}_{1.233}O_4 \xrightarrow{\Delta} 0.985Li^{+}_{1.06}Ni^{2+}_{0.01}Mn^{3+}_{0.8}Mn^{4+}_{1.13}O_4 + 0.030O_2 \quad (7)$$

$$Li^{+}_{1.053}Cr^{3+}_{0.0099}Mn^{3+}_{0.755}Mn^{4+}_{1.163}O_4 \xrightarrow{\Delta} 0.994Li^{+}_{1.06}Cr^{3+}Mn^{3+}_{0.81}Mn^{4+}_{1.12}O_4 + 0.013O_2 \quad (8)$$

$$Li^{+}_{1.051}Co^{3+}_{0.0093}Mn^{3+}_{0.742}Mn^{4+}_{1.172}O_4 \xrightarrow{\Delta} 0.992Li^{+}_{1.06}Co^{3+}_{0.01}Mn^{3+}_{0.81}Mn^{4+}_{1.12}O_4 + 0.015O_2 \quad (9)$$

It is worth to note that the Ni^{2+} and Al^{3+}-doped spinels, which undergo a weight loss in the 380–680 °C interval higher than the Cr^{3+} and Co^{3+}-doped ones, have been synthesized using a smaller amount of sugar (1.5*w*) than the latter (3*w*). It points out that the amount of sugar used in the synthesis influences both the particle size and the stoichiometry of the "as prepared" spinels.

For temperature higher than 720 °C decomposition of the spinel starts off and a continuous weight loss takes place up to 1000 °C. This weight loss is ascribed to oxygen removal, and it was already confirmed by mass spectrometry analysis of the gases evolved during the thermal analysis of the samples [23,24]. Having in mind the thermal behavior of the "as prepared samples", they were then thermally treated at 700 °C for 1 h, to get stoichiometric spinels.

XRD patterns of the samples heated in air at 700 °C are similar. They show relatively sharp diffraction lines that evidence better structural perfection than the "as prepared" samples. Patterns recorded for the $LiMn_{1.99-y}Li_yM_{0.01}O_4$ (M = Ni^{2+}, Al^{3+}; $y = 0.01$ and 0.06) spinels are shown in Fig. 3, as an example. All diffraction peaks can be indexed in the Fd3m space group, spinel-type structure, indicating that we are dealing with single-phase spinels. This result demonstrates that the sucrose-aided synthesis procedure is very well adapted for the synthesis of pure doubly-doped $LiMn_2O_4$-based spinels. Lattice parameter determined for all the 700 °C-treated samples are presented in Table 1. It is observed that, in general, the lattice parameters of the 700 °C-treated Ni^{2+} and Al^{3+}-doped spinels are slightly larger than those of the "as prepared" samples, i.e. they increases after the thermal treatment, while those for the Cr^{3+} or Co^{3+}-doped spinels remain practically constant. This effect is consistent with the formulation proposed in Eqs. (6)–(9). At ≈400 °C the Mn^{4+} content in the "as-prepared" Ni^{2+} and Al^{3+}-doped samples is higher than in the "as-prepared" Cr^{3+} and Co^{3+} ones, i.e. the amount of Mn^{4+} reduced to Mn^{3+} is higher in the former samples than in the latter ones. The increase of the fraction of Mn^{3+} ions, whose ionic radius [34] is larger than that of Mn^{4+}, accounts for the observed increase in the lattice parameter. It can be concluded that the Co^{3+} and Cr^{3+}-doped samples, which have been prepared using a larger amount of fuel, 3*w*, seem to be more "stoichiometric" than the Ni^{2+} and Al^{3+}-doped spinels, which have been synthesizing by using a smaller amoun of fuel, 1.5*w*.

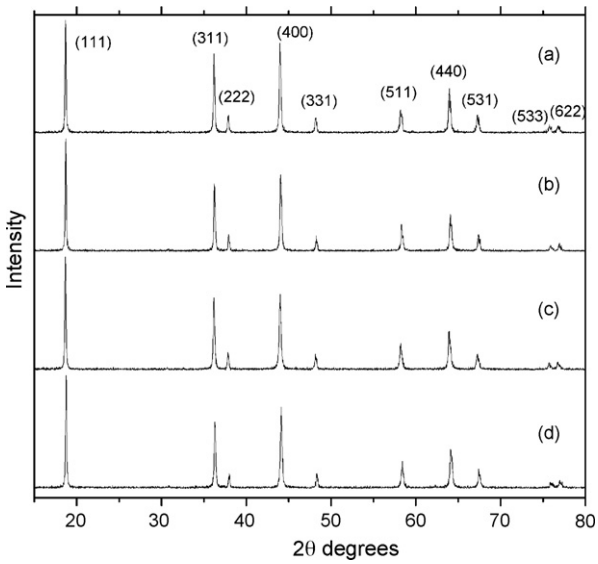

Fig. 3. Room temperature XRD patterns of some 700°-heated $LiMn_{1.99-y}Li_yM_{0.01}O_4$ spinels: (a) $LiMn_{1.98}Li_{0.01}Ni_{0.01}O_4$, (b) $LiMn_{1.93}Li_{0.06}Ni_{0.01}O_4$, (c) $LiMn_{1.98}Li_{0.01}Al_{0.01}O_4$, (d) $LiMn_{1.93}Li_{0.06}Al_{0.01}O_4$.

The crystallite size determined by the Scherrer equation for the 700 °C-heated samples is summarized in Table 1. It is worth to remark that in all cases we are dealing with nanometric materials. The small particle size shown by the $LiMn_{1.99-y}Li_yM_{0.01}O_4$ synthesized by the sucrose-aided combustion procedure can be accounted for considering that gases evolved during the combustion produce the reaction mass to spread out, and makes the reaction product to be made of loosely-packed particles. The heat developed during the burning is also dissipated by the gaseous products, hindering the sintering of the particles. As it was observed for the "as prepared" spinels, samples containing Cr^{3+} and Co^{3+} have crystallite size (≈40 nm) smaller than those doped with Al^{3+} and Ni^{2+} (≈60 nm). This result shows that spinels obtained with larger amount of fuel (Cr^{3+} and Co^{3+}-doped spinels) have slightly smaller crystallite size than those synthesized using less amount of fuel (Al^{3+} and Ni^{2+}-doped spinels). In a previous paper we synthesized singly doped $LiM_yMn_{2-y}O_4$ spinels (M = Co^{3+}, Cr^{3+} and Ni^{2+}) using the same amount of sugar [13]. Independently of the M-dopant cation, the 700 °C-heated samples showed practically the same crystallite size, indicating that the particle size is not influenced by the dopant cation. Hence, in the present paper differences observed in crystallite size have been ascribed to the different amounts of sugar used in the synthesis. Transmission electron micrographs of the 700 °C-heated spinels were also taken. As an example, images of the $LiMn_{1.98}Li_{0.01}Al_{0.01}O_4$, $LiMn_{1.93}Li_{0.06}Al_{0.01}O_4$ and $LiMn_{1.93}Li_{0.06}Co_{0.01}O_4$ samples are shown in Fig. 4a–c; the corresponding particle size histograms are presented at the right part

Table 1
Lattice parameter and crystallite size determined for the "as prepared" and the 700 °C-heated $LiMn_{1.99-y}Li_yM_{0.01}O_4$ (M = Ni^{2+}, Al^{3+}, Cr^{3+}, Co^{3+}, $y = 0.01, 0.06$) spinels.

Nominal composition	400 °C		700 °C	
	Lattice parameter a_c (Å)	Crystallite size (nm)	Lattice parameter a_c (Å)	Crystallite size (nm)
$LiMn_{1.98}Li_{0.01}Ni_{0.01}O_4$	8.221(7)	18	8.2332(3)	62(4)
$LiMn_{1.93}Li_{0.06}Ni_{0.01}O_4$	8.204(4)	19	8.2168(3)	66(4)
$LiMn_{1.98}Li_{0.01}Al_{0.01}O_4$	8.221(4)	20	8.2316(4)	55(5)
$LiMn_{1.93}Li_{0.06}Al_{0.01}O_4$	8.211(6)	17	8.2151(4)	58(5)
$LiMn_{1.98}Li_{0.01}Cr_{0.01}O_4$	8.230(8)	23	8.2345(9)	37(3)
$LiMn_{1.93}Li_{0.06}Cr_{0.01}O_4$	8.223(2)	23	8.2245(6)	39(4)
$LiMn_{1.98}Li_{0.01}Co_{0.01}O_4$	8.234(2)	23	8.2349(9)	39(4)
$LiMn_{1.93}Li_{0.06}Co_{0.01}O_4$	8.221(2)	22	8.2243(7)	41(4)

$Ni^{2+}$and Al^{3+}-doped samples have been synthesized with 1.5 w amount of sugar, Cr^{3+}, Co^{3+} samples have been synthesized with 3w amount of sugar.

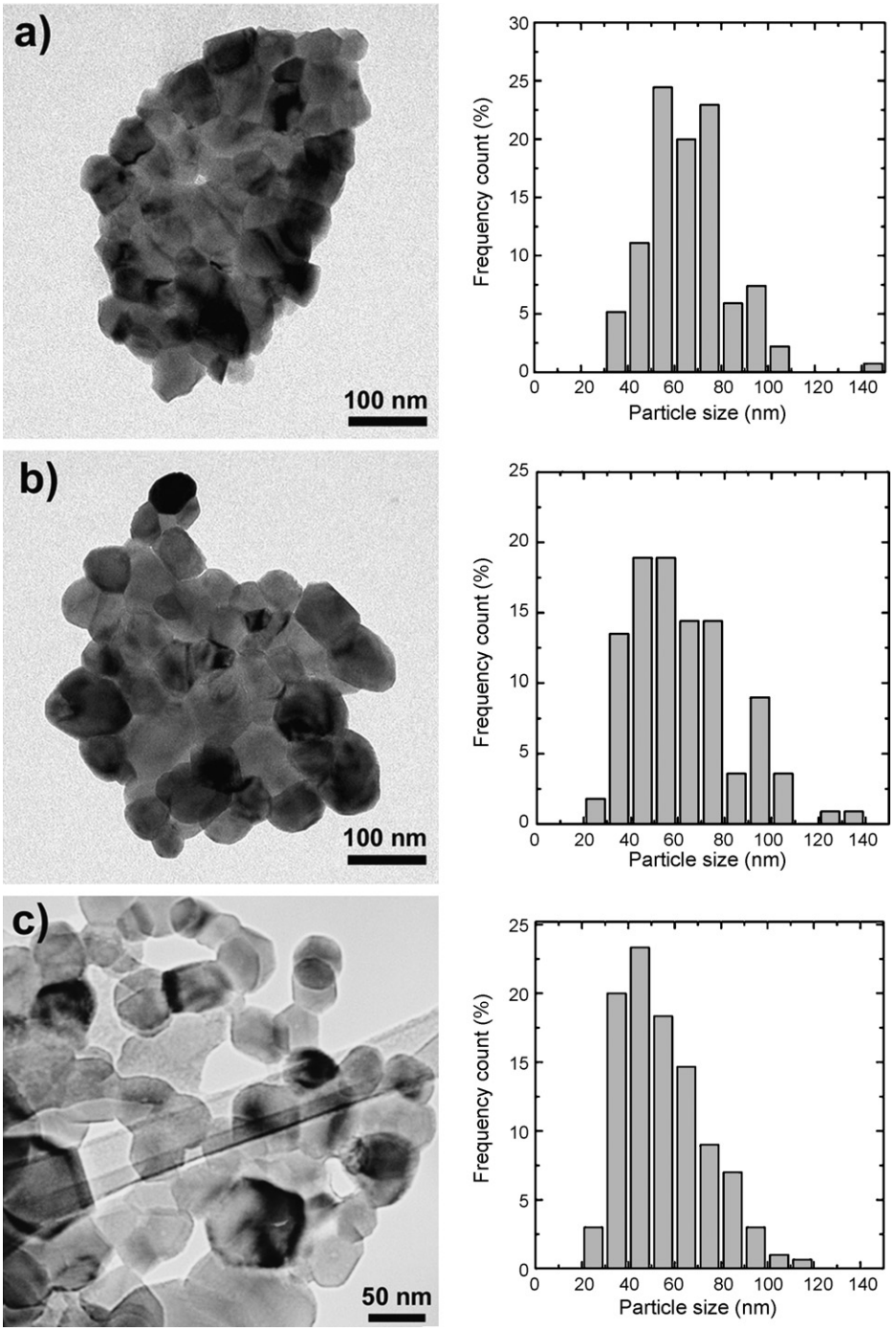

Fig. 4. TEM micrographs of some 700 °C-heated $LiMn_{1.99-y}Li_yM_{0.01}O_4$ spinels: (a) $LiMn_{1.98}Li_{0.01}Al_{0.01}O_4$, (b) $LiMn_{1.93}Li_{0.06}Al_{0.01}O_4$, (c) $LiMn_{1.93}Li_{0.06}Co_{0.01}O_4$; the corresponding particle size histograms are presented at the right part of each micrograph.

of this figure. For all the samples the micrographs show a homogeneous distribution of the faceted units. It is observed that the increase of Li-dopant (Fig. 4a and b) does not affect the size of the particles. Both Al^{3+}-doped samples have an average particle size of ≈60 nm, which fairly agrees with the values determined from XRD analysis. However, the amount of fuel used in the synthesis does affect the particle size. In effect, the histogram of the $LiMn_{1.93}Li_{0.06}Co_{0.01}O_4$ spinel, that has been obtained with larger amount of fuel ($3w$) than the Al^{3+}-doped spinels ($1.5w$), show that particles are smaller, ≈40 nm, in agreement with the values determined by the Scherrer method.

3.2. Electrochemical properties

Electrochemical studies were performed on the 700 °C-heated $LiMn_{1.99-y}Li_yM_{0.01}O_4$ (M = Al^{3+}, Ni^{2+}, Cr^{3+} and Co^{3+}, y = 0.01, 0.06) spinels at 25 and at 55 °C. The first charge/discharge curves of samples registered at high currents (0.5C/1C charge/discharge rates) in the 4 V region for the $LiMn_{1.99-y}Li_yCr^{3+}{}_{0.01}O_4$ at 25 °C and for the $LiMn_{1.99-y}Li_yAl^{3+}{}_{0.01}O_4$ at 55 °C, y = 0.01 and 0.06, are plotted in Fig. 5a and b respectively, as an example. Curves recorded both at 25 and at 55 °C for the y = 0.01 spinels (dotted line) clearly show the two plateaus observed for stoichiometric $LiMn_2O_4$ spinel [1,4,10,35]. For

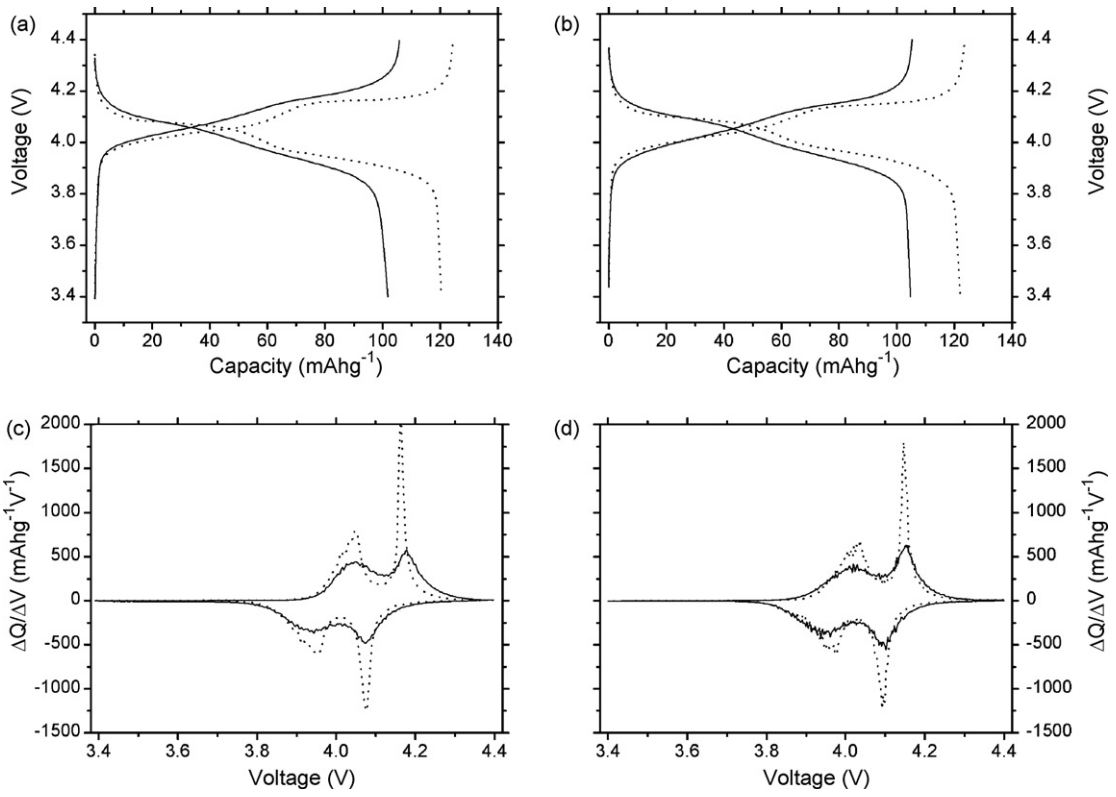

Fig. 5. First charge/discharge curves of the 700 °C-heated spinels: (a) $LiMn_{1.99-y}Li_yCr_{0.01}O_4$ at 25°, (b) $LiMn_{1.99-y}Li_yAl_{0.01}O_4$ at 55 °C, $y = 0.01$ (dotted line), $y = 0.06$ (straight line); corresponding derivative curves: (c) $LiMn_{1.99-y}Li_yCr_{0.01}O_4$ at 25 °C, (d) $LiMn_{1.99-y}Li_yAl_{0.01}O_4$ at 55 °C; $y = 0.01$ (dotted line), $y = 0.06$ (straight line).

the $y = 0.06$ spinels (straight line), the curves are more sloped and the two plateaus are less defined. Moreover, the plateaus developed at high voltage are L-shaped for the $y = 0.01$ samples and S-shaped for the $y = 0.06$ spinels. Differences between samples with different Li-excess is general for all the samples studied in this work, independently of the transition metal dopant, the fuel content and the working temperature. More detailed information about the Li^+ de/insertion processes can be extracted from the corresponding derivative curves plotted in Fig. 5c and d. The derivative curves for the $y = 0.01$ samples at 25 and at 55 °C show a first broad peak at ≈4.05 V in charge and ≈3.95 V in discharge, and a second very sharp peak, at ≈4.16 V in charge and ≈4.08 V in discharge. For the $y = 0.06$ spinels these two peaks are clearly observed at about the same potentials. Moreover, the peak at high potential is significantly broader than the one observed for the $y = 0.01$ samples. This variation in the shape of the curves suggests that the Li^+ de/insertion mechanism in the high voltage plateau changes for all the samples on increasing the Li-excess. A similar behavior has been reported by Xia and Yoshio [36] for $Li_{1+y}Mn_{2-y}O_4$ spinels. The authors have demonstrated by XRD that the Li^+ de/insertion mechanism in the high voltage region changes from a two phase reaction for stoichiometric $LiMn_2O_4$, to a one phase reaction for Li-rich $Li_{1+y}Mn_{2-y}O_4$. The increase of the average oxidation state of Mn on increasing the Li-excess explains the change observed in the mechanism.

The values of the discharge capacity, Q_d, determined for each spinel, are gathered together with the calculated theoretical

Table 2
Theoretical discharge capacity (Q_{theor}), discharge capacity (Q_d), capacity loss (Q_d/Q_{theor}), capacity retention after 100 cycles (QRt-100) and cyclability (cc) of the 700 °C-heated $LiMn_{1.99-y}Li_yM_{0.01}O_4$ (M = Al^{3+}, Ni^{2+}, Cr^{3+}, Co^{3+}; $y = 0.01$ and 0.06) spinels synthesized by the sucrose-aided combustion method.

Working temperature (°C)	Composition	Q_{theor} (mAh g^{-1})	Q_d (mAh g^{-1})	Q_d/Q_{theor} (%)	QRt-100 (%)	cc (% by cycle)
25	$LiMn_2O_4$	148.2	128.9	87	86.9	99.84
	$LiMn_{1.98}Li_{0.01}Al_{0.01}O_4$	142.9	121.1	85	94.9	99.94
	$LiMn_{1.98}Li_{0.01}Ni_{0.01}O_4$	141.2	121.1	86	95.3	99.96
	$LiMn_{1.98}Li_{0.01}Cr_{0.01}O_4$	142.7	120.4	84	92.5	99.95
	$LiMn_{1.98}Li_{0.01}Co_{0.01}O_4$	142.6	121.7	85	92.5	99.93
	$LiMn_{1.93}Li_{0.06}Al_{0.01}O_4$	122.20	104.0	85	95.8	99.94
	$LiMn_{1.93}Li_{0.06}Ni_{0.01}O_4$	120.5	105.1	87	96.4	99.97
	$LiMn_{1.93}Li_{0.06}Cr_{0.01}O_4$	122.0	101.8	84	94.3	99.95
	$LiMn_{1.93}Li_{0.06}Co_{0.01}O_4$	122.0	104.3	85	93.2	99.94
55	$LiMn_2O_4$	148.2	124.5	84	74.3	99.70
	$LiMn_{1.98}Li_{0.01}Al_{0.01}O_4$	142.9	122.9	86	83.2	99.84
	$LiMn_{1.98}Li_{0.01}Ni_{0.01}O_4$	141.2	120.0	85	85.4	99.85
	$LiMn_{1.98}Li_{0.01}Cr_{0.01}O_4$	142.7	117.1	82	78.4	99.78
	$LiMn_{1.98}Li_{0.01}Co_{0.01}O_4$	142.6	121.7	85	79.9	99.80
	$LiMn_{1.93}Li_{0.06}Al_{0.01}O_4$	122.2	105.7	86	90.4	99.91
	$LiMn_{1.93}Li_{0.06}Ni_{0.01}O_4$	120.5	105.3	87	90.7	99.92
	$LiMn_{1.93}Li_{0.06}Cr_{0.01}O_4$	122.0	103.0	85	86.82	99.88
	$LiMn_{1.93}Li_{0.06}Co_{0.01}O_4$	122.0	105.0	86	86.8	99.87

capacity, Q_{theor}, in Table 2. Q_{theor} has been calculated assuming that Mn^{3+} is the only active cation in the 4 V region [1]. The amount of Mn^{3+} in our spinels was calculated by the general equation: $Mn^{3+} = 1\text{-}3y\text{-}(4\text{-}n)z$; where y stands for the Li-excess, n and z are the charge and the amount of the M^{n+} dopant cation ($z = 0.01$), respectively. Data for undoped $LiMn_2O_4$ synthesized by the sugar-aided combustion method, with 38(4) nm particle size, has been included for comparison. It is observed that for all the spinels, Q_d is ≈85% of the Q_{theor} (Table 2). This capacity diminution (≈15%), which is similar for all samples, can be ascribed to the way of preparation of the cathode composite. With the wet method used, some of the particles of the active material are fully coated with the plasticizer. Then, they are electrically isolated and inactive for the Li^+ de/insertion reaction. This result agrees with previous measurements done on $LiMn_2O_4$ cathodes prepared by dry mixing and grinding [37] or by a wet procedure used in this work. The dry procedure yields pellets with poor mechanical properties, but with a capacity at $C/12$ rate of 135 mAh g^{-1}, which is higher than the one obtained when the cathodes are prepared by the wet method [30], 120 mAh g^{-1}.

Discharge capacities, Q_d, for the $LiMn_{1.98}Li_{0.01}M_{0.01}O_4$ ($y = 0.01$) measured at 25 and at 55 °C are ≈120 mAh g^{-1}, while those for the $LiMn_{1.93}Li_{0.06}M_{0.01}O_4$ ($y = 0.06$) are ≈105 mAh g^{-1} (Table 2). Thus, Q_d clearly depends on the Li-excess and it is not affected by the metal dopant or the working temperature. Q_d is also independent as well on the different particle size shown by the samples synthesized with different amount of sugar (Table 1). Having in mind the calculated percentage of capacity loss due to the isolated particles (≈15%), the measured Q_d are very close to the theoretical ones. It is worth to remark that the measurements have been done at high currents ($0.5C/1C$ charge/discharge rates), so the likeness between Q_{theor} and Q_d is indicative of the good rate capability shown by these spinels (Table 2).

The long-term cyclability of the spinels at 25 and at 55 °C, and the influence of the composition and particle size on the capacity retention have also been examined. Fig. 6 shows the evolution of the discharge capacity vs. cycle number at 25 and at 55 °C for the $LiMn_{1.99-y}Li_yM_{0.01}O_4$ ($y = 0.01$ and 0.06, open and closed symbols, respectively). From these data the capacity retention after 100 cycles, QRt-100, and the cyclability, cc, calculated with the equation $Q_n = Q_1 cc^{(n-1)}$ have been determined (Table 2). At 25 °C QRt-100 and the cc of the $LiMn_{1.99-y}Li_yM_{0.01}O_4$ spinels for both $y = 0.01$ and 0.06 are very high, (QRt-100 > 92% and cc > 99.90% by cycle). In all cases, they are higher than those determined for $LiMn_2O_4$ (Fig. 6a, Table 2), and they are among the best values reported in the literature for $LiMn_2O_4$-based cathodes [10,13,15,38–40]. It is worth to mention that at 55 °C the $y = 0.06$ spinels also show good capacity retention (Fig. 6b, Table 2). Values of QRt-100 > 90% and cc > 99.9% by cycle have been observed for the $LiMn_{1.93}Li_{0.06}M_{0.01}O_4$, ($M = Al^{3+}, Ni^{2+}$, $y = 0.06$) spinels. These values are higher than the ones shown by the $y = 0.01$ spinels, (QRt-100 ≈ 80%, cc ≈ 99.8%), or by undoped $LiMn_2O_4$, (QRt-100 = 74.3%, cc = 99.70%). Moreover, the $LiMn_{1.93}Li_{0.06}M_{0.01}O_4$, ($M = Al^{3+}$, Ni^{2+}) spinels also have better cycling performance at high temperature than the ones reported by Shin and Manthiram [10], for doped $LiMn_2O_4$-based cathodes having similar Mn average oxidation state.

To investigate the possible causes of the variation of the cycling performance at 25 and 55 °C, we have first analyzed if some structural alteration could be at the origin of the capacity fade observed. We have recorded the XRD patterns of the cathode composites before and after 100 cycles. As an example, the patterns recorded for the $LiMn_{1.99-y}Li_yCr_{0.01}O_4$ ($y = 0.01$ and 0.06) cathode pellets before and after cycling at 55 °C are shown in Fig. 7. The patterns after 100 cycles do not show any peaks others than those of the pristine spinels indicating that the structure is kept along the cycling and that no any crystalline impurities are formed. Similar results

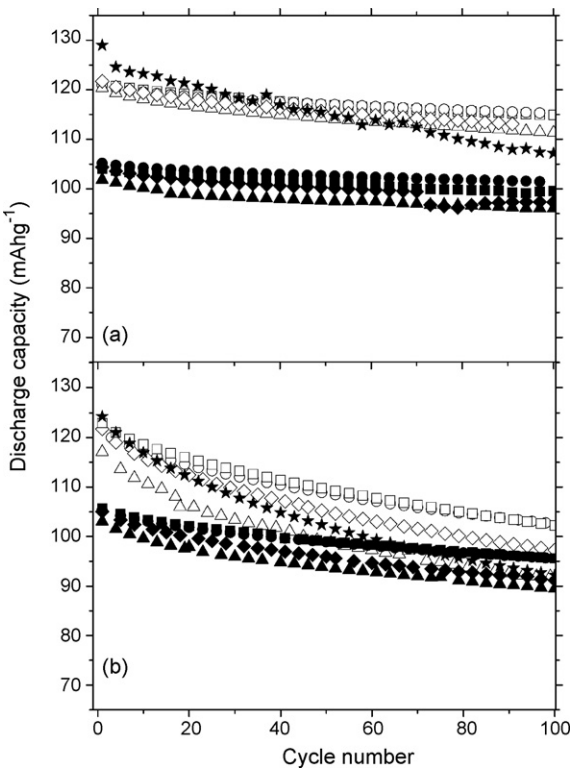

Fig. 6. Cycling behaviour of the 700 °C-heated $LiMn_{1.99-y}Li_yM_{0.01}O_4$ spinels at: (a) 25 °C; (b) 55 °C. M = Ni^{2+} (○,●), Al^{3+}(□, ■), Cr^{3+} (△, ▲), Co^{3+} (◊, ♦). Open and closed symbols stand for the $y = 0.01$ and $y = 0.06$ spinels, respectively, $LiMn_2O_4$ (⋆) as reference.

are obtained for all the other M^{n+} doping cations. These results reveal that the observed diminution of capacity cannot be justified based on some structural feature. Having in mind that one of the main factors proposed to explain the observed capacity fade of the $LiMn_2O_4$-based electrodes is the dissolution of the pristine spinel in the electrolyte [5–7], the diminution observed in the capacity retention between 25 and 55 °C, particularly for the $y = 0.01$ samples, could be due to an increase of the spinels dissolution at high temperature. To evaluate this hypothesis, the derivative curves for

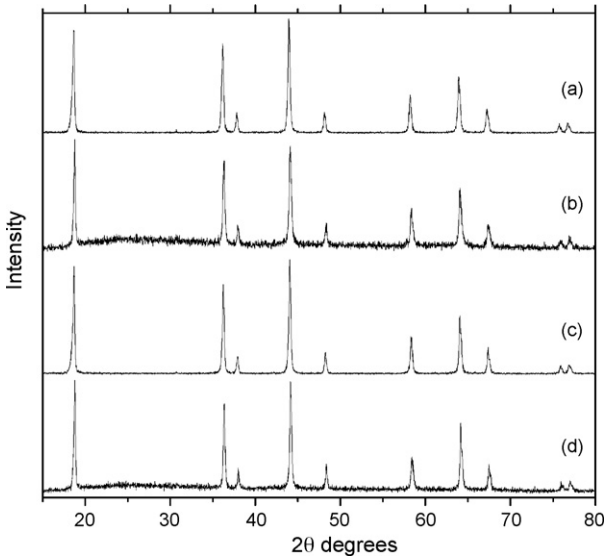

Fig. 7. Room temperature XRD patterns of the $LiMn_{1.99-y}Li_yCr_{0.01}O_4$ pellet cathodes: before [$y = 0.01$(a); $y = 0.06$(c)] and after 100 cycles at 55 °C [$y = 0.01$(b); $y = 0.06$(d)].

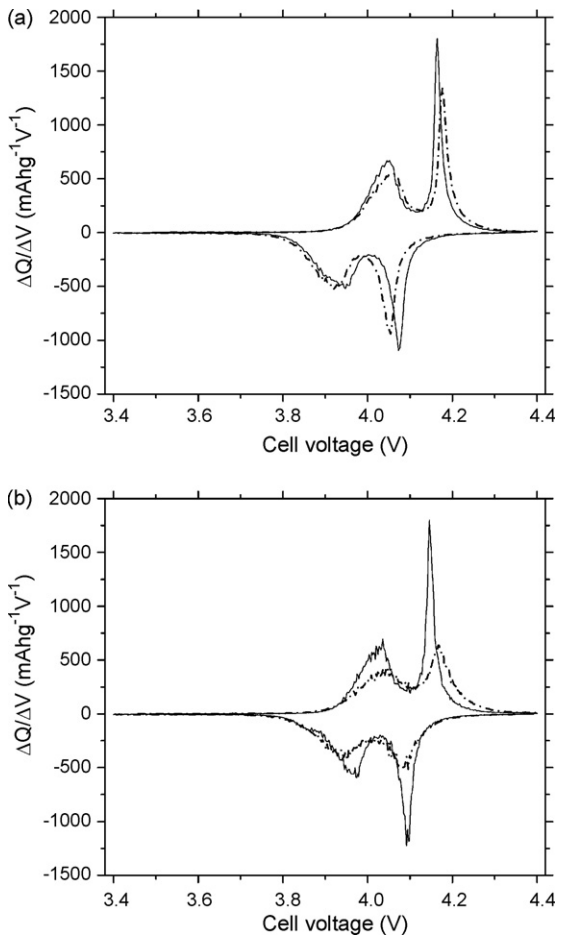

Fig. 8. Derivative curves of the 1st (solid line) and 100th (dash-dot line) cycles of $LiMn_{1.98}Li_{0.01}Al_{0.01}O_4$: (a) at 25 °C; (b) at 55 °C.

the 1st and 100th cycle of the $LiMn_{1.98}Li_{0.01}Al_{0.01}O_4$ ($y = 0.01$) at 25 and at 55 °C are compared in Fig. 8. At 25 °C, the high potential peak at ≈4.15/4.1 V in charge/discharge for both the 1st and the 100th cycles is sharp (Fig. 8a). It indicates that in this case, there is no change in the Li^+ de/insertion mechanism on cycling. However, at 55 °C this sharp peak transforms into a broad peak after 100 cycles (Fig. 8b). This transformation shows that a change from a two-phase mechanism to a one-phase mechanism has taken place. Xia et al. [41] observed a similar change of the mechanism during cycling of the $LiMn_2O_4$ at 50 °C, which was explained by the dissolution of Mn. Accordingly, at 25 °C the dissolution of the $LiMn_{1.98}Li_{0.01}Al_{0.01}O_4$ spinel if any, is so small that it does not affect the cycling behaviour (the mechanism does not change). However at 55 °C the amount of Mn dissolved must be notably higher than at 25 °C since it provokes the change in the Li-de/insertion mechanism. Thus, the higher dissolution at 55 °C accounts for the diminution observed in the capacity retention between 25 and 55 °C.

In Fig. 9, plot of the variation of QRt-100 vs. particle size for the $LiMn_{1.99-y}Li_yM_{0.01}O_4$ (M = Al^{3+}, Ni^{2+}, Cr^{3+}, Co^{3+}; $y = 0.01, 0.06$) spinels is presented. It can be seen that QRt-100 increases on increasing the particle size. This effect can be explained by the dissolution of the spinels, which must be lower for the samples having larger particle size [42,43]. The analysis of the plot shows that the variation of QRt-100 with the particle size also depends on the Li excess and on the working temperature. At 25 °C (closed symbols in Fig. 9) QRt-100, changes very slightly with the Li excess. Assuming a linear increase of QRt-100 with the particle size, the slopes of the $y = 0.01$ and $y = 0.06$ spinels are small and very close, +0.12 and +0.10, respectively. At 55 °C (open symbols in Fig. 9) the effect of

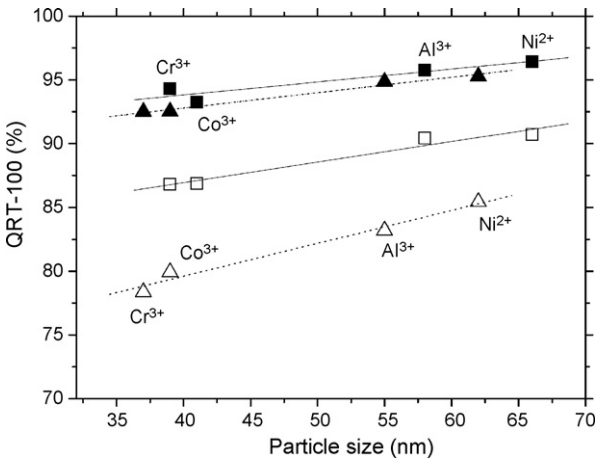

Fig. 9. Capacity retention after 100 cycles (QRt-100) vs. Scherrer particle size for the 700 °C-heated $LiMn_{1.98}Li_yM_{0.01}O_4$ (Al^{3+}, Ni^{2+}, Cr^{3+}, Co^{3+}; $y = 0.01, 0.06$) cycled at 25° (closed symbols) and at 55 °C (open symbols); $y = 0.01$ (▲, △), $y = 0.06$ (■, □). (The straight lines are the linear fittings).

the Li excess is more relevant that at 25 °C. In fact, the slope of the $y = 0.06$ spinels (+0.16) is higher than the one determined at 25 °C, and it notably increases up to +0.26 for the $y = 0.01$ samples. This variation of the slopes shows that cycling behavior of the $y = 0.06$ spinels are less affected by the increase of the particle size. In agreement with this result, Yoshio et al. [16] showed that the dissolution

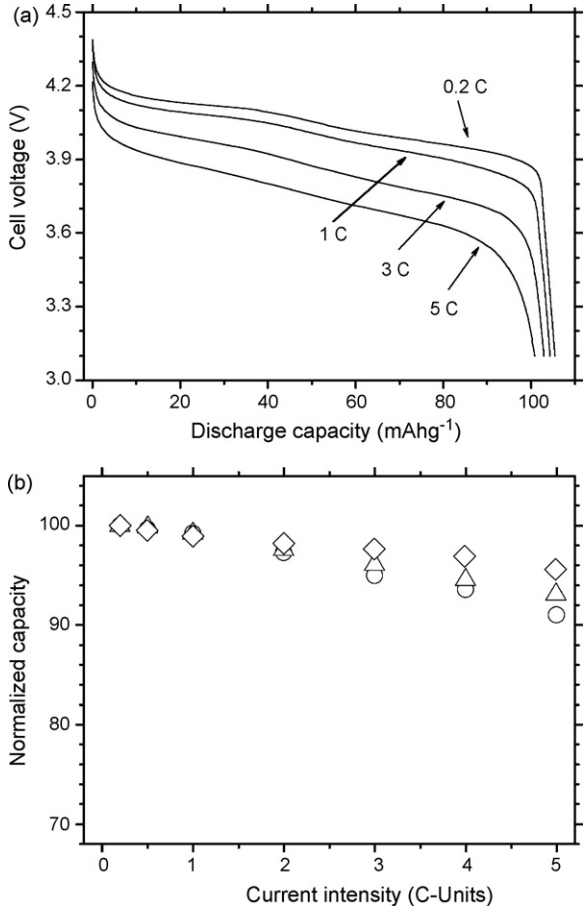

Fig. 10. (a) discharge curves of the $LiMn_{1.93}Li_{0.06}Co_{0.01}O_4$ spinel registered at the indicated increasing rates; (b) comparison of the rate capability (i.e. capacity vs rate) of cathodes comprising nanosize $LiMn_{1.98}Li_{0.01}Co_{0.01}O_4$ (△), $LiMn_{1.93}Li_{0.06}Co_{0.01}O_4$ (◊), $LiMn_{1.93}Li_{0.06}Al_{0.01}O_4$ spinels (○).

of the Li, Cr doped $LiMn_2O_4$ decreases on increasing the amount of dopant cations. In our case, the variation of the spinel dissolution due to differences in particle size and in Li excess explain the observed evolution of QRt-100. Moreover, this result indicates that the simultaneous increase of particle size and Li excess has a synergic effect that improves the high temperature cycling performances of the $LiMn_2O_4$ based cathodes.

The rate capability of $LiMn_{1.99-y}Li_yM_{0.01}O_4$ electrodes has been also investigated. As an example, discharge curves for $LiMn_{1.93}Li_{0.06}Co_{0.01}O_4$ spinel registered at increasing rates are compared in Fig. 10a. The curves have similar shape; in fact, the two plateaus are evident even at 3*C* rate. On increasing the intensity current, the potentials of the plateaus decrease due to polarization effects, but capacities at the end of discharge are close. The Q_d only decrease from 105 mAh g^{-1} to 101 mAh g^{-1}, in spite that discharge rate has increased more than 20 times, from 0.2*C* to 5*C*. In Fig. 10b, the evolution of the normalized capacity Q_{nor} vs. rate for electrodes comprising the $LiMn_{1.98}Li_{0.01}Co_{0.01}O_4$, $LiMn_{1.93}Li_{0.06}Co_{0.01}O_4$ and $LiMn_{1.93}Li_{0.01}Al_{0.06}O_4$ spinels is compared. In all cases, the capacity decreases slightly on increasing the rate but even at 5*C*, Q_{nor} is >90% of the capacity drained at low current (0.2*C*). The values measured for these spinels are similar to those reported by Shin and Manthiram [10] for the doubly doped $LiMn_{2-2y}Li_yNi_yO_4$ spinels, and higher than the reported for single doped $LiMn_{2-y}M_yO_4$ spinels [10]. All these results permit us to conclude that $LiMn_{1.99-y}Li_yM_{0.01}O_4$ ($M = Al^{3+}$, Ni^{2+}, Cr^{3+}, Co^{3+}; $y = 0.01, 0.06$) spinels synthesized by the combustion method show an excellent rate capability. The nanometric size of the samples obtained by the combustion method explains the high rate capability of the synthesized spinels.

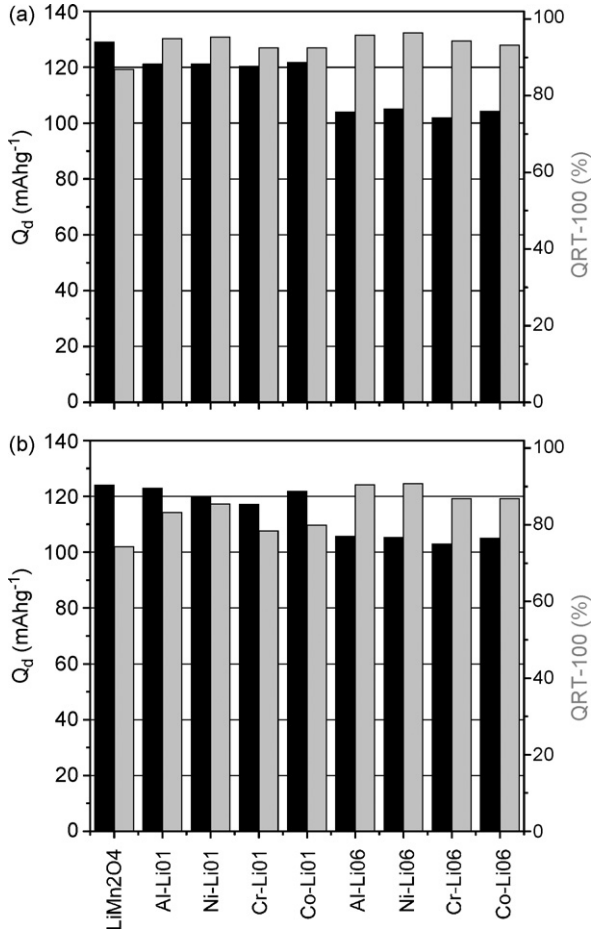

Fig. 11. Discharge capacity (Q_d) and capacity retention after 100 cycles (QRt-100) for the $LiMn_{1.99-y}Li_yM_{0.01}O_4$ ($y = 0.01$ and 0.06) spinels at: (a) 25 °C; (b) 55 °C.

Finally, the electrochemical performances, i.e. the discharge capacity (Q_d) and the cycling performance (QRt-100) at 25 and at 55 °C for all the $LiMn_{1.99-y}Li_yM_{0.01}O_4$ spinels synthesized have been compared in Fig. 11. Data for undoped $LiMn_2O_4$ have been also included. It can be seen that at 25 °C the low-doped $LiMn_{1.98}Li_{0.01}M_{0.01}O_4$ spinels ($y = 0.01$) are the ones that clearly show the best electrochemical performances (Fig. 11a). They show the highest capacity and their cycling behaviour is close to the one shown by the $y = 0.06$ spinels, and remarkable better than those of $LiMn_2O_4$. For instance, at 25 °C the spinel with composition $LiMn_{1.98}Li_{0.01}Ni_{0.01}O_4$, which is the one that shows the largest particle size (≈60 nm), has $Q_d = 121$ mAh g^{-1}, QRt-100 = 95.3%, and ciclability of 99.96% by cycle (Fig. 11a, Table 2). At 55 °C the choice is not so evident, albeit the capacity of the $y = 0.01$ spinels is higher than that of the $y = 0.06$ spinels (Table 2), the ciclability of the latter is higher than that of the former (Fig. 11b). So, in our opinion, the $LiMn_{1.93}Li_{0.06}Ni_{0.01}O_4$ and $LiMn_{1.93}Li_{0.06}Al_{0.01}O_4$, that have capacities of ≈105 mAh g^{-1} and ciclabilities of ≈99.9% by cycle, are the two spinels that better fulfil both capacity and cycling performance requirements at high temperature. It is worth to mention that the Q_d and cc values shown by these samples are among the best reported for $LiMn_2O_4$-based spinels [10,13,15,38–40], indicating that they are very well suited materials for application as cathode in Li-ion batteries working even at high temperature. Furthermore, the remarkable rate capability exhibited by the $LiMn_{1.99-y}Li_yM_{0.01}O_4$ spinels, coupled with the low cost and low toxicity of these compounds, makes them very attractive for hybrid and electric vehicles.

4. Conclusions

The sucrose aided combustion synthesis is an attractive, powerful and straightforward method for the synthesis of nanosized $LiMn_2O_4$-based spinels with complex composition, as the $LiMn_{1.99-y}Li_yM_{0.01}O_4$ (M = Al, Ni, Cr, Co, $y = 0.01, 0.06$) compounds synthesized in this work. Our results point out that the amount of fuel (sucrose) in the reaction mixture controls the particle size and the composition of the "as prepared" spinels. Further thermal treatment at 700 °C of the "as prepared" samples yields pure and stroichiometric spinels. XRD and TEM studies show that all the spinels synthesized have nanometric particle size that slightly increases on decreasing the amount of fuel used in the synthesis. The discharge capacity Q_d shown at high current (1*C* rate) by the spinels studied in this work decreases on increasing the Li-excess, but it does not change with the metal dopant, the amount of fuel or the working temperature. At room temperature all the spinels studied have a very good cycling performance, with high capacity retention after 100 cycles, QRt-100 ≥ 92% and ciclability cc ≥ 99.9% by cycle. At high temperature, 55 °C, the $y = 0.06$ spinels also show a good capacity retention, QRt-100 ≥ 86%, being it higher than the ones shown by the $y = 0.01$ spinels, QRt-100 ≈ 81%. Differences in the cycling performances have been related to different solubility of the spinels in the electrolyte. The analysis of the evolution of QRt-100 vs. particle size shows that the simultaneous increase of particle size and the Li-excess has a synergic effect that improves the high temperature cyclablility of the samples synthesized. The $LiMn_{1.99-y}Li_yM_{0.01}O_4$ ($y = 0.01$, 0.06) retain >90% of the capacity even at 5*C* rate. The nanometric particle size of the spinels can account for this remarkable rate capability. Among the spinels synthesized, the $LiMn_{1.93}Li_{0.06}M_{0.01}O_4$, $M = Al^{3+}$, Ni^{2+}, with a potential ≈4 V, capacity ≈105 mAh g^{-1}, ciclabilities >99.9% at both 25 and 55 °C, and high rate capabilities, are the ones that show the best electrochemical properties. These qualities, together with the low cost and low toxicity of these compounds, make them very attractive materials as cathodes for Li-ion batteries with applications in hybrid and electric vehicles.

Acknowledgements

Financial support through project MAT 2008-03182 (MICINN), and the joint project CSIC-Bulgarian Academy of Sciences no. 2007BG0018 is gratefully recognized.

References

[1] M.M. Thackeray, Progr. Solid State Chem. 25 (1997) 1.
[2] L.A.H. MacLean, C. Poinsignon, J.M. Amarilla, F. Le Cras, P. Strobel, J. Mater. Chem. 5 (1995) 1183.
[3] M.M. Thackeray, in: J.O. Besenhard (Ed.), Handbook of Battery Materials, Wiley-VCH, 1999, pp. 293–321.
[4] Y. Xia, M. Yoshio, in: G.A. Nazri, G. Pistoia (Eds.), Lithium Batteries: Science and Technology, Kluwer Academic Publishers, 2004, pp. 361–380.
[5] E. Iwata, K. Takahashi, K. Maeda, T. Mouri, J. Power Sources 81–82 (1999) 430.
[6] H. Yamane, T. Inoue, M. Fujita, M. Sano, J. Power Sources 99 (2001) 60.
[7] J.-S. Kim, J.T. Vaughey, C.S. Johnson, M.M. Thackeray, J. Electrochem. Soc. 150 (2003) A1498.
[8] M.M. Thackeray, Y. Shao-Horn, A.J. Kahaian, K.D. Kepler, E. Skinner, J.T. Vaughey, S.A. Hackney, Electrochem. Solid State Lett. 1 (1998) 7.
[9] Y. Shin, A. Manthiram, Electrochem. Solid State Lett. 5 (2002) A55.
[10] Y. Shin, A. Manthiram, Chem. Mater. 15 (2003) 2954.
[11] P. Arora, B.N. Popov, R.E. White, J. Electrochem Soc. 145 (1998) 807.
[12] G.X. Wang, D.H. Bradhurst, H.K. Liu, S.X. Dou, Solid State Ionics 120 (1999) 95.
[13] J.M. Amarilla, R.M. Rojas, F. Picó, L. Pascual, K. Petrov, D. Kovacheva, M.G. Lazarraga, I. Lejona, J.M. Rojo, J. Power Sources 174 (2007) 1212.
[14] C. Bellitto, E.M. Bauer, G. Righini, M.A. Green, W.R. Branford, A. Antonini, M. Pasquali, J. Phys. Chem. Solids 65 (2004) 29.
[15] Y. Shin, A. Manthiram, J. Electrochem. Soc 151 (2004) A204.
[16] M. Yoshio, Y. Xia, N. Kumada, S. Ma, J. Power Sources 101 (2001) 79.
[17] A. Yamada, J. Solid State Chem. 122 (1996) 160.
[18] H. Ikuta, K. Takanaka, M. Wakihara, Thermochim. Acta 414 (2004) 227.
[19] J. Molenda, D. Palubiak, J. Marzec, J. Power Sources 144 (2005) 176.
[20] J.M. Amarilla, R.M. Rojas, J. Thermal Analysis Cal. 73 (2003) 191.
[21] Y. Shin, A. Manthiram, Electrochem. Solid State Lett. 6 (2003) A34.
[22] D. Kovacheva, H. Gadjov, K. Petrov, S. Mandal, M.G. Lazarraga, L. Pascual, J.M. Amarilla, R.M. Rojas, P. Herrero, J.M. Rojo, J. Mater. Chem. 12 (2002) 1184.
[23] M.G. Lazarraga, L. Pascual, H. Gadjov, D. Kovacheva, K. Petrov, J.M. Amarilla, R.M. Rojas, M.A. Martín-Luengo, J.M. Rojo, J. Mater. Chem. 14 (2004) 1640.
[24] L. Pascual, H. Gadjov, D. Kovacheva, K. Petrov, P. Herrero, J.M. Amarilla, R.M. Rojas, J.M. Rojo, J. Electrochem. Soc. 152 (2005) A301.
[25] C.R. Sides, N. Li, C.J. Patrissi, B. Scrosati, C.R. Martin, MRS Bull. 27 (2002) 604.
[26] A. Singhal, G. Skandan, G. Amatucci, F. Badway, N. Ye, A. Manthiram, H. Ye, J.J. Xu, J. Power Sources 129 (2004) 38.
[27] A.S. Aricó, P.G. Bruce, B. Scrosati, J.M. Tarascon, W. van Schalkwijk, Nat. Mater. 4 (2005) 366.
[28] R.M. Rojas, J.M. Amarilla, L. Pascual, J.M. Rojo, D. Kovacheva, K. Petrov, J. Power Sources 160 (2006) 529.
[29] J. Laugier, A. Filhol, CelRef, PC version (unplished) ILL, Grenoble, France, 1991.
[30] M.G. Lazarraga, S. Mandal, J. Ibáñez, J.M. Amarilla, J.M. Rojo, J. Power Sources 115 (2003) 315.
[31] A. de Koch, M.H. Rossouw, L.A. de Picciotto, M.M. Thackeray, Mater. Res. Bull. 25 (1990) 657.
[32] P. Strobel, A. Ibarra Palos, M. Anne, J. Power Sources 97–98 (2001) 381.
[33] T. Tsang, A. Manthiram, Solid State Ionics 89 (1996) 305.
[34] D. Shannon, Acta Crystallogr. A32 (1976) 751.
[35] L. Pascual, M.L. Pérez-Revenga, R.M. Rojas, J.M. Rojo, J.M. Amarilla, Electrochim. Acta 51 (2006) 3193.
[36] Y. Xia, M. Yoshio, J. Electrochem. Soc. 143 (1996) 825.
[37] S. Mandal, J.M. Amarilla, J. Ibañez, J.M. Rojo, J. Electrochem. Soc. 148 (2001) A24.
[38] K. Ariyoshi, E. Iwata, M. Kuniyoshi, H. Wakabayashi, T. Ohzuku, Electrochem, Solid State Lett. 9 (2006) A560.
[39] R. Koksbang, J. Barker, H. Shi, M.Y. Saidi, Solid State Ionics 84 (1996) 1.
[40] G. Amatucci, J.-M. Tarascon, J. Electrochem. Soc. 149 (2002) K31.
[41] Y. Xia, Y. Zhou, M. Yoshio, J. Electrochem. Soc. 144 (1997) 2593.
[42] Y. Xia, N. Kumada, M. Yoshio, J. Power. Sources 90 (2000) 135.
[43] B. Deng, H. Nakamura, Q. Zhang, M. Yoshio, Y. Xia, Electrochim. Acta 49 (2004) 1823.